TR-SAR: TIME REVERSAL TARGET FOCUSING IN SPOTLIGHT SAR

Yuanwei Jin and José M.F. Moura

Carnegie Mellon University
Department of Electrical and Computer Engineering
Pittsburgh, PA 15213

ABSTRACT

We develop *time reversal* spotlight synthetic aperture radar (TR-SAR) for target focusing and ghost images removal in SAR. Conventional SAR is not designed for imaging targets in a rich scattering environment. In this case, ghost images due to secondary reflections appear in the SAR images. We show in this paper, how, from a rough estimate of the target location obtained from a conventional SAR image and using time reversal, TR-SAR focuses on the target with improved resolution, and reduces or removes ghost images. Verification with experimentally measured electromagnetic data demonstrates the success of TR-SAR.

Index Terms— Synthetic aperture radar, imaging

1. INTRODUCTION

Synthetic aperture radar (SAR) images a target region reflectivity function in the multi-dimensional spatial domain of range and cross range [1]. SAR synthesizes a large aperture radar. The cross range resolution of the SAR is $R\lambda/D$, where D is the synthetic aperture, R is the target range, and λ is the wavelength of the measured waveform.

When imaging a target, the conventional SAR theory does not include the effects of multiple scattering from the surrounding objects in a high clutter area. In addition to the true target image, multiple-bounce echoes caused by surrounding scatterers produce spurious and random patterns in the formed SAR image. We refer to these as ghost images. A common practice to distinguish the true target from its ghost images is leading edge detection, i.e., if the ghost image is caused by trailing echoes, we may identify the peak that has the shortest range as the target. However, unless we know *a priori* where the scatterers are, or what their physical characteristics are, it is difficult to distinguish the true target from the ghost images.

In this paper, we combine time reversal with synthetic aperture radar (TR-SAR) to reduce or remove ghost patterns and form a clean target map in a high clutter scene. Furthermore, once we identify a target spot, we can examine the shape or the size of the target with *improved* resolution. Time reversal is well known for its temporal and spatial focusing in highly cluttered environments [2, 3, 4]. Experiments have demonstrated that time reversal produces a higher resolution that exceeds the Rayleigh limit. We develop here methodologies and algorithms that form *cleaner* and *higher* resolution images by time reversal than conventional SAR.

This work is funded by the Defence Advanced Research Projects Agency through the Army Research Office under grant no. W911NF-04-1-0031.

In TR-SAR, we process the data in two steps: conventional step and time reversal step. The conventional step is conventional SAR processing and produces images that contain the target as well as the ghost patterns. The time reversal step focuses on the dominant patterns and provides higher resolution. Focusing on a chosen pattern with high resolution resembles a camera zooming on a particular spot to see the details of its structure. The details may be the size or the shape of the target. If the focused spot has a target, we can recognize its shape or its size. However, if the focused spot is a ghost pattern, the details are blurred and random, and do not resemble any particular object. Thus, we are able to distinguish the target from its ghost patterns. To further improve the accuracy of the initial estimate of the location of a fixed target from the conventional SAR images, we can average a number of SAR images taken from different look angles. Due to the randomness of the appearance of the ghost patterns in SAR images, the averaging enhances the intensity of the target spot while reducing the intensity of the ghost patterns.

2. DESCRIPTION OF TR-SAR

We illustrate the algorithm with a bistatic SAR. Bistatic radar employs two sites. The target is illuminated by the transmitter at one site, while the target echoes are detected and processed by the receiver at the second site. Fig. 1 depicts the geometry of the bistatic spotlight SAR. A moving transmit antenna, denoted by the letter A, synthesizes an aperture $u \in [-L, L]$ with total size $2L$. The center of the aperture is chosen to be the origin in the Cartesian coordinate system. The y-axis is along the aperture direction u. A fixed antenna, denoted by the letter B, is at (X_B, Y_B). The target area is $[X_c - X_0, X_c + X_0] \times [Y_c - Y_0, Y_c + Y_0]$ and centered at (X_c, Y_c). The n-th scatterer (or target) coordinates are $(X_c + x_n, Y_c + y_n)$.

2.1. Time reversal data collection

The proposed bistatic time reversal SAR is as follows.

Step-1: Clutter probing In this case, the target is not present, and we measure the clutter response. Antenna A moves along the y-axis with coordinates $(0, u)$, where $u \in [-L, L]$. It transmits a waveform $P(\omega)$ with bandwidth Ω. The returned signal at antenna B is

$$S_c(\omega, u) = P(\omega) G_c(\omega; \mathbf{r}, \mathbf{r}_u) G_c(\omega; \mathbf{r}_B, \mathbf{r}), \qquad (1)$$

where $G_c(\omega; \mathbf{r}, \mathbf{r}_u)$ and $G_c(\omega; \mathbf{r}_B, \mathbf{r})$ are the Green's functions of the clutter between the aperture location $\mathbf{r}_u$, the ground

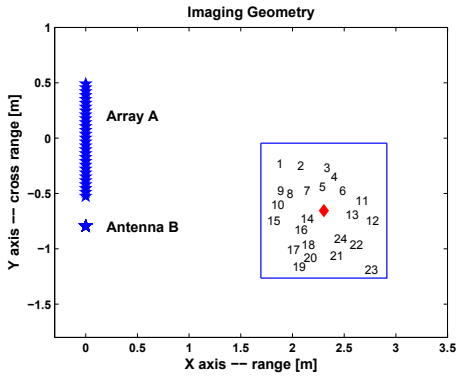

Fig. 1. Geometry of bistatic spotlight SAR in squint mode: array A with aperture $u \in [-L, L]$ is centered at the origin, and antenna B is at a fixed location (X_B, Y_B). The ground patch is centered at (X_c, Y_c) (denoted by the diamond) with its boundary indicated by the large square. The numbers indicate the scatterer locations.

patch location $\mathbf{r}$, and the antenna B location $\mathbf{r}_B$. We adopt the spherical phase function employed in conventional SAR theory, i.e., $G_c(\omega; \mathbf{r}_1, \mathbf{r}_2) = \frac{1}{|\mathbf{r}_1 - \mathbf{r}_2|} e^{-jk|\mathbf{r}_1 - \mathbf{r}_2|}$. Note that $G_c(\omega; \mathbf{r}_B, \mathbf{r})$ is not a function of u. For a stationary area, it is possible to estimate the clutter response by collecting a large amount of samples at frequency ω and aperture u. Hence we assume that $S_c(\omega, u)$ is known.

Step-2: Target probing The target is now present. The target is masked by the clutter. Antenna A moves along the same aperture path $u \in [-L, L]$ and transmits the same type of signal $P(\omega)$ as it does in Step-1. The returned signal is recorded at antenna B

$$S_{t+c}(\omega, u) = P(\omega) G_{t+c}(\omega; \mathbf{r}, \mathbf{r}_u) G_{t+c}(\omega; \mathbf{r}_B, \mathbf{r}), \quad (2)$$

where $G_{t+c}(\omega; \mathbf{r}, \mathbf{r}_u)$ and $G_{t+c}(\omega; \mathbf{r}_B, \mathbf{r})$ are the Green's functions of the target plus the clutter between the aperture at $\mathbf{r}_u$, the ground patch at $\mathbf{r}$, and antenna B at $\mathbf{r}_B$.

Step-3: Time reversal We subtract out the clutter component

$$S(\omega, u) = S_{t+c}(\omega, u) - S_c(\omega, u). \quad (3)$$

In an ideal case, (3) performs the background subtraction, and the signal scattered by the clutter is removed. Therefore, (3) is the effective target response. In practice, however, clutter can not be removed completely by simple subtraction. The residual clutter response results in phase errors in the SAR data. Phase error correction, for example, autofocus techniques, must be employed. In this paper, we assume that the clutter reflections can be removed via (3).

Up to now, the processing steps will be common to both SAR and TR-SAR. For SAR, the signal $S(\omega, u)$ is used to produce conventional SAR images. For TR-SAR, the residual signal $S(\omega, u)$ is time-reversed (or phase conjugated in the frequency domain), energy normalized by $\eta(u)$, where $\eta(u) = \sqrt{\int |P(\omega)|^2 d\omega} / \sqrt{\int |S(\omega, u)|^2 d\omega}$, and re-transmitted back to the target area. In reality, we do not need to actually re-transmit the time reversed signal but perform mathematical time reversal (see, e.g., [4]). The re-transmitted signal from antenna B back to antenna A, denoted by $Z(\omega, u)$, is given by

$$Z(\omega, u) = \eta(u) S^*(\omega, u). \quad (4)$$

Step-4: TR-SAR processing The received signal at antenna A takes the form of

$$R_{t+c}(\omega, u) = Z(\omega, u) G_{t+c}(\omega; \mathbf{r}_u, \mathbf{r}) G_{t+c}(\omega; \mathbf{r}, \mathbf{r}_B). \quad (5)$$

We then subtract out the clutter component

$$R_c(\omega, u) = Z(\omega, u) G_c(\omega; \mathbf{r}_u, \mathbf{r}) G_c(\omega; \mathbf{r}, \mathbf{r}_B), \quad (6)$$

which yields the residue signal

$$R(\omega, u) = R_{t+c}(\omega, u) - R_c(\omega, u). \quad (7)$$

Again, the subtraction in (7) may not cancel out all the clutter response, which may result in phase errors. The phase errors can cause image degradation and must be corrected in subsequent processing steps. We assume here that the residual clutter response is negligible. Next, the signal (7) undergoes TR-SAR processing to produce images as explained in the following section.

2.2. Time reversal SAR processing

Conventional SAR performs matched filtering in both the fast time domain (range) and the slow time domain (cross range). In high clutter, the target response consists of the direct path echo and the multiple bounce echoes caused by the secondary scattering. In the development of the TR-SAR processing, we assume that the clutter component has been subtracted out from the measurements. In what follows, we focus on the residue target response that contains the direct path and the secondary paths. For simplicity, we consider a two path model for the moment. It is straightforward to extend to the multiple path model. For a single target located at $(X_c + x_n, Y_c + y_n)$, we let

$$\begin{aligned} R_n(u) &= \sqrt{(X_c + x_n)^2 + (Y_c + y_n - u)^2} + \\ &\quad \sqrt{(X_c + x_n - X_B)^2 + (Y_c + y_n - Y_B)^2} \end{aligned}$$

denote the distance between the aperture at $(0, u)$, the target, and antenna B at (X_B, Y_B). The received signal from the target can be written as

$$S(\omega, u) = P(\omega) \tau_n \left(e^{-jk R_n(u)} + \alpha e^{-jk \overline{R}_n(u)} \right), \quad (8)$$

where τ_n is the reflectivity function of the n-th target. $\overline{R}_n(u)$ denotes the second path caused by the scattering environment. The parameter α represents the attenuation for the second path relative to the direct path. The wavenumber is $k = \omega / c$. For a conventional SAR, the measurement in (8) undergoes matched filtering by the reference signal

$$S_0(\omega, u) = P(\omega) e^{-jk R_0(u)}, \quad (9)$$

where

$$\begin{aligned} R_0(u) &= \sqrt{X_c^2 + (Y_c - u)^2} + \\ &\quad \sqrt{(X_c - X_B)^2 + (Y_c - Y_B)^2}. \end{aligned} \quad (10)$$

The compressed data after matched filtering become

$$S(\omega,u)S_0^*(\omega,u) = |P(\omega)|^2\tau_n\left(e^{-jk[R_n(u)-R_0(u)]}+ \alpha e^{-jk[\overline{R}_n(u)-R_0(u)]}\right) \quad (11)$$

$$= |P(\omega)|^2\tau_n e^{-jk[R_n(u)-R_0(u)]} + |P(\omega)|^2\tau_n\alpha e^{-jk[\overline{R}_n(u)-R_0(u)]}. \quad (12)$$

In SAR, the first term in (12) corresponds to the target image, while the second term corresponds to the ghost pattern.

For the time reversal SAR, the to-be-transmitted time reversed signal is

$$S^*(\omega,u) = \eta(u)P^*(\omega)\tau_n\left(e^{jkR_n(u)} + \alpha^* e^{jk\overline{R}_n(u)}\right). \quad (13)$$

The returned echo is

$$S^{\text{tr}}(\omega,u) = S^*(\omega,u)\tau_n\left(e^{-jkR_n(u)} + \alpha e^{-jk\overline{R}_n(u)}\right). \quad (14)$$

Next, we choose one spot to focus on. From the images provided by conventional SAR, we have a rough estimate of the target location $(\widehat{x}_n, \widehat{y}_n)$, for example, by choosing the leading pattern, or a dominant pattern. The initial estimate of the target location can also be obtained by searching along the range of the image and identifying the leading spot that exceeds a threshold. Thus, we calculate the target distance $\widehat{R}_n(u)$ as

$$\widehat{R}_n(u) = \sqrt{(X_c+\widehat{x}_n)^2+(Y_c+\widehat{y}_n-u)^2} + \sqrt{(X_c+\widehat{x}_n-X_B)^2+(Y_c+\widehat{y}_n-Y_B)^2}.$$

Next, we choose the following reference signal for the subsequent TR-SAR processing

$$\widehat{S}_0(\omega,u) = \left[P(\omega)e^{jk\widehat{R}_n(u)}\right]e^{-jkR_0(u)}. \quad (15)$$

This choice of reference signal implies that, in TR-SAR, we match the received data with the signal $P(\omega)e^{jk\widehat{R}_n(u)}$. The last term $e^{-jkR_0(u)}$ is common for conventional SAR. The compressed data take the form of

$$S^{\text{tr}}(\omega,u)\widehat{S}_0^*(\omega,u) = \eta(u)|P(\omega)|^2|\tau_n|^2 e^{-jk\widehat{R}_n(u)}e^{jkR_0(u)} \left(e^{jkR_n(u)} + \alpha^* e^{jk\overline{R}_n(u)}\right)\left(e^{-jkR_n(u)} + \alpha e^{-jk\overline{R}_n(u)}\right),$$

$$= \eta(u)|P(\omega)|^2|\tau_n|^2\phi(\omega,u) e^{-jk(R_n(u)-R_0(u))}, \quad (16)$$

where

$$\phi(\omega,u) = \left(e^{jk(R_n(u)-\widehat{R}_n(u))} + \alpha^* e^{jk(\overline{R}_n(u)-\widehat{R}_n(u))}\right)\left(1+\alpha e^{-jk(\overline{R}_n(u)-R_n(u))}\right). \quad (17)$$

We now examine (16) and (17). Suppose that the estimate $(\widehat{x}_n, \widehat{y}_n)$ is accurate, i.e., $\widehat{R}_n(u) = R_n(u)$. This leads to

$$\phi(\omega,u) = \left|1+\alpha e^{-jk(\overline{R}_n(u)-R_n(u))}\right|^2. \quad (18)$$

We note that $\phi(\omega,u)$ is the *focusing gain* in time reversal at frequency ω and aperture u. Further inspection of (18) reveals that, for a general multiple path model with echoes $\sum_i^N \alpha_i e^{-jk\overline{R}_{n,i}(u)}$, where N is the number of dominant paths, α_i is the i-th attenuation, the gain is given by

$$\phi_N(\omega,u) = \left|1+\sum_{i=1}^{N}\alpha_i e^{-jk(\overline{R}_{n,i}(u)-R_n(u))}\right|^2. \quad (19)$$

To illustrate the potential gain in (19), assuming that $\alpha_i = 1$, $k(\overline{R}_{n,i}(u) - R_n(u)) = i\Delta\phi$, we can then simplify (19) as a sinc-like function proportional to the number of paths, N,

$$\phi_N(\omega,u) = \left|\frac{1-e^{-jN\Delta\phi}}{1-e^{-j\Delta\phi}}\right|^2 = N^2\left|\frac{\text{sinc}\left[\frac{N\Delta\phi}{2\pi}\right]}{\text{sinc}\left[\frac{\Delta\phi}{2\pi}\right]}\right|^2. \quad (20)$$

Thus, given the compressed data in (16), a final image is then produced by taking the inverse Fourier Transform of (16) [1]:

$$f(x,y) = \int_\omega\int_{k_u} d\omega dk_u e^{jk_x(\omega,k_u)x+jk_y(\omega,k_u)y}J(\omega,k_u) |P(\omega)|^2|\tau_n|^2\mathcal{F}_{(u)}\left[\eta(u)\phi(\omega,u)e^{-jk(R_n(u)-R_0(u))}\right], \quad (21)$$

where $J(\omega,k_u)$ is the Jacobian of the transformation from $[k_x(\omega,k_u), k_y(\omega,k_u)]$ to (ω,k_u). Due to space limitations, we omit the details leading to (21).

3. EXPERIMENTS AND RESULTS

To test our analysis, we performed electromagnetic measurements in a laboratory environment. The geometry is shown in Fig. 1. The target is a single copper pipe with 1.5 cm in diameter and 2.5 m in length. The scatterers are dielectric pipes with 3 cm in diameter and 2.5 m in length. Besides the dielectric pipes, we add a few copper pipes as scattering objects. Two dielectric pipes are wrapped with aluminum foils to increase the reflectivity. All the pipes stand vertically. We use two horn antennas operating in the frequency range $4-6$ GHz (wavelength of the center frequency $\lambda_c = 6$ cm), one for transmitting and one for receiving. Antenna A moves along a slider to synthesize a synthetic aperture of about 1 meter long. We take 30 positions with an increment of 3.5 cm. Antenna B is at a fixed location. Both antennas are elevated to about 1.2 meters above ground. Thus, we measure the cylindrical wave propagating between the antennas and the scattering objects. During the measuring process, the two horn antennas point to the target area centered at $(X_c, Y_c) = (2.3, -0.65)$ meter of size 1.2 meter by 1.2 meter. This is the spotlight mode in a bistatic configuration. We extract the SAR signature of the targeted area by range and cross range gating. We use the range stacking algorithm described in [1] to implement SAR.

Figs. 2 depicts the conventional SAR image and the TR-SAR image. In all the images, the shorter and thicker cross indicates the exact target location, while the larger cross represents the peak of the image. Numbers indicate the locations of the scatterers. The conventional SAR image, the uppermost figure in Fig. 2, shows numerous ghost patterns, the peak of

the image is far away from the target location. The bias is about 22.2 cm (about $3.7\lambda_c$). By choosing the closest pattern in range, we obtain the target estimate of $(2.3, -0.6)$ meters. The TR-SAR is shown in the middle figure. The ghost patterns are clearly removed in the TR-SAR image. The bias is reduced to 3.6 cm (or $0.6\lambda_c$). If we carry out the peak picking technique in conventional SAR processing, i.e., we use $S_0(\omega, u) = P(\omega)e^{-jk\widehat{R}_n(u)}e^{-jkR_0(u)}$ instead of (9), we obtain an image shown in the lower figure in Fig. 2. The image quality is very poor.

To examine the resolution, we project the SAR image (uppermost figure) and TR-SAR image (the middle figure) onto range and cross range, as shown in the lowest figure in Fig. 2. The cross range resolution (-3 dB) for TR-SAR reads as 17 cm compared with 23 cm for SAR. The range resolution that is governed by the bandwidth of the system remains the same, about 12 cm. The TR-SAR image clearly has a smaller sidelobe level than the SAR image.

4. CONCLUSION

A multipath rich scattering environment results in ghost patterns in conventional SAR images. In this paper, we combined time reversal with synthetic aperture radar to image a single target in high clutter. The proposed TR-SAR forms a cleaner target image with improved resolution than conventional SAR. Focusing on the target spot with higher resolution allows us to further examine the size or the shape of the target. We carried out electromagnetic experiments in a laboratory environment to verify our analysis. The results demonstrated the success of TR-SAR. In future research, we will develop phase correction techniques applicable to the TR-SAR algorithm, and will carry out a robustness analysis in the case of incomplete clutter cancellation or wrong estimation of the initial target location.

5. ACKNOWLEDGEMENT

The authors thank Yi Jiang for help with getting some of the experimental electromagnetic data in section 3.

6. REFERENCES

[1] M. Soumekh, *Synthetic Aperture Radar Signal Processing*. New York, NY: John Wiley & Sons, Inc., 1999.

[2] M. Fink, "Time reversed acoustics," *Physics Today*, vol. 50, no. 3, pp. 34–40, 1997.

[3] J. M. F. Moura, Y. Jin, D. Stancil, J. Zhu, A. Cepni, Y. Jiang, and B. Henty, "Single antenna time reversal adaptive interference cancelation," in *ICASSP'05, IEEE International Conference on Signal Processing*, vol. IV. Philadelphia, PA: IEEE, March 2005, pp. 1121–1124.

[4] J. M. F. Moura and Y. Jin, "Detection by time reversal: single antenna," *IEEE Transactions on Signal Processing*, vol. 55, no. 1, pp. 187–201, January 2007.

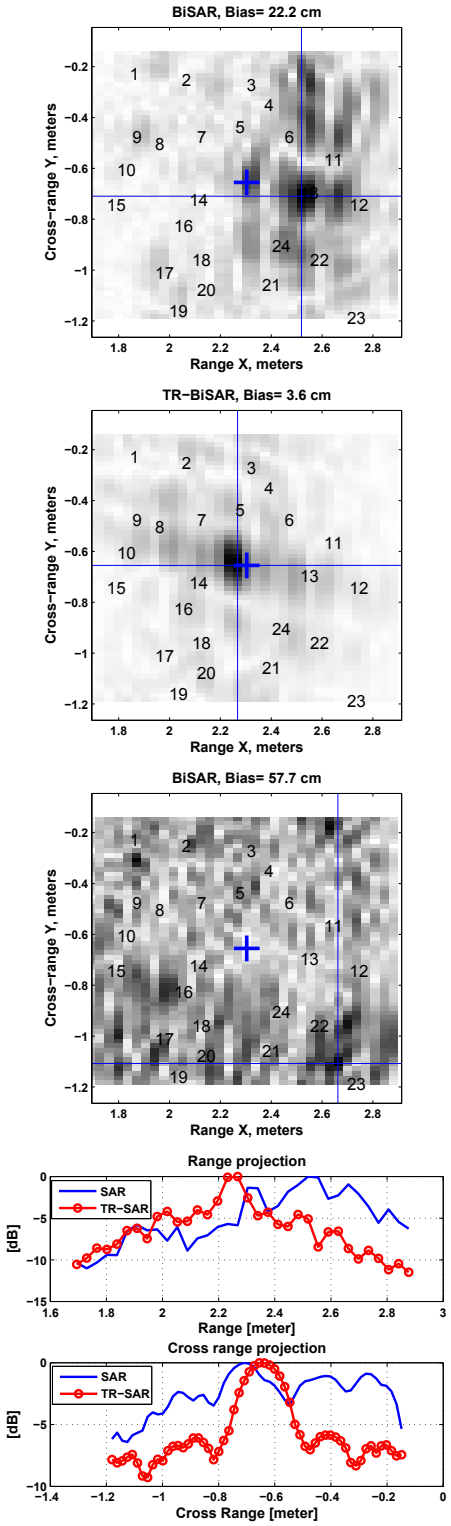

Fig. 2. Uppermost figure – conventional SAR image with ghost patterns. Middle figure – TR-SAR image. Lower figure – conventional SAR with peak picking technique. Lowest figure – range and cross range resolution plots. The shorter and thicker cross indicates the exact target location, the larger cross represents the peak of the image.